Analyst

DNA Target Parameters for Sensitive Hybridization-induced Aggregation of Particles for the Sequence-specific Detection of DNA

Journal:	*Analyst*
Manuscript ID:	AN-ART-11-2014-002101.R1
Article Type:	Paper
Date Submitted by the Author:	14-Jan-2015
Complete List of Authors:	Landers, James; University of Virginia, Department of Chemistry Leslie, Dan; Harvard, Wyss Inst Lee, Jacob; VCU, Chemistry Sloane, Hillary; University of Virginia, Chemistry Strachan, Briony; University of Houston, Biomedical Engineering

Revised submission to

Analyst

Investigation of the DNA Target Design Parameters for Effective Hybridization-induced Aggregation of Particles for the Sequence-specific Detection of DNA

Briony C. Strachan[1], Hillary S. Sloane[1], Jacob C. Lee[1] Daniel C. Leslie[1] and James P. Landers[1,2,3]

[1]Dept of Chemistry, University of Virginia, Charlottesville, VA 22904

[2]Dept of Pathology, University of Virginia Health Science Center, Charlottesville, VA 22908

[3]Dept of Mechanical Engineering, University of Virginia, Charlottesville, VA 22904

Graphical Abstract:

An investigation into target DNA characteristics for the label-free detection of ssDNA via hybridization-induced aggregation (HIA).

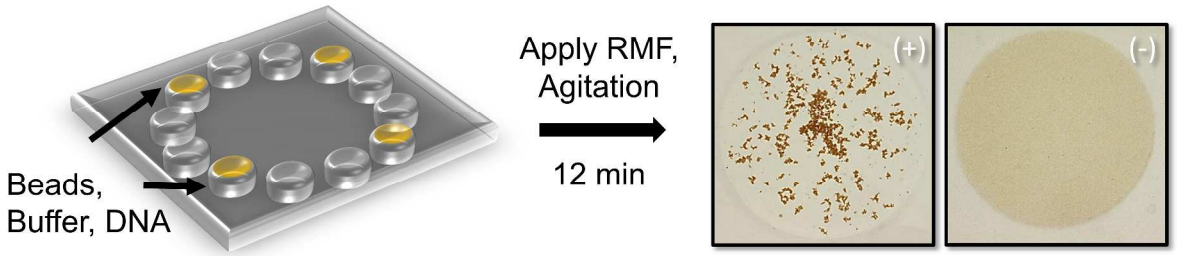

Abstract

In a recent publication, we presented a label-free method for the detection of specific DNA sequences through the hybridization-induced aggregation (HIA) of a pair of oligonucleotide-adducted magnetic particles. Here we show, through the use of modified hardware, that we are able to simultaneously analyze multiple (4) samples, and detect a 26-mer ssDNA sequence at femtomolar concentrations in minutes. As such, this work represents an improvement in throughput and a 100-fold improvement in sensitivity, compared to that reported previously. Here, we also investigate the design parameters of the target sequence, in an effort to maximize the sensitivity of HIA to use as a guide in future applications of this work. Modifications were made to the original 26-mer oligonucleotide sequence to evaluate the effects of: 1) non-complementary flanking bases, 2) target sequence length, and 3) single base mismatches on aggregation response. The aggregation response decreased as the number of the non-complementary flanking bases increased, with only a five base addition lowering the LOD by four orders of magnitude. Low sensitivity was observed with short sequences of 6 and 10 complementary bases, which were only detectable at micromolar concentrations. Target sequences with 20, 26 or 32 complementary bases provided the greatest sensitivity and were detectable at femtomolar concentrations. Additionally, HIA could effectively differentiate sequences that were fully complementary from those containing 1, 2 or 3 single base mismatches at micromolar concentrations. The robustness of the HIA system to other buffer components was explored with nine potential assay interferents that could affect hybridization (aggregation) or falsely induce aggregation. Of these, purified BSA and lysed whole blood induced a false aggregation. None of the interferents inhibited aggregation when the hybridizing target was added. Having delineated the fundamental parameters affecting HIA-target hybridization, and

demonstrating that HIA had the selectivity to detect single base mismatches, this fluor-free end-point detection has the potential to become a powerful tool for microfluidic DNA detection.

Keywords: hybridization; aggregation; rotating magnetic field; DNA

Introduction

The interrogation of genomic DNA for specific sequences is essential for most biological assays, certainly for clinical diagnostics, functional genomics, food safety and even for forensic analysis. The specificity needed for most DNA assays relies on hybridization, with an almost exponential improvement in sensitivity since Ed Southern described the Southern blot in the mid-1970's [1]. The sensitivity of assays, the mass of target (or number of copies) required to produce a signal distinguishable from noise, is often driven by improvements in detection hardware, with concurrent increase in complexity and cost and, usually, with the read-out based on fluorescence [2-4].

Hybridization-based detection often involves the binding of DNA to a complementary oligonucleotide probe(s) attached to a surface. The use of paramagnetic particles (PMPs) as a vehicle for the probe has proliferated since Mirkin, *et al.* developed colorimetric detection of DNA hybridization with gold nanoparticles in 1996 [5, 6]. The properties of nanoparticles have since been further exploited with more sophisticated DNA detection modalities. Included in these are Raman spectroscopy [7, 8], electrical stimulation [9, 10], electrophoresis [11] and optical detection. These range from simplistic, cost-effective methods like colorimetric assays [12, 13], to the more complex microfabrication-dependent systems like cantilever deflection [14].

Effective DNA hybridization is essential for sensitive detection, regardless of the platform. This includes the use of the appropriate buffer components, temperature, mechanism of probe mobilization [15], DNA/probe concentration, kinetics [16], and assay duration. In addition, successful hybridization is dependent on the nucleic acid composition of the DNA sequence (or 'target' sequence), itself. Generally, the target is prepared such that the resulting target:probe hybridization complex is completely complementary, with no additional, unhybridized bases [17].

However, deviations from this convention have been successfully demonstrated with some target designs. Scanometric technology, for example, allowed for 10 pM detection with the hybridization of a 48-base target sequence, where the target had 10 non-complementary bases flanking each end of the probed sequence [18]. In addition, the length of the target is also significant, as secondary structural effects increase with length, and this can decrease sensitivity [19]. Ultimately, optimization of the sequence design allows for the most specific and sensitive assay.

Identification of single point mutations (SPM's) is one of the major driving forces in the development of hybridization assay technology. Since the hybridization of a target DNA sequence containing a point mutation, or mismatch, is thermodynamically less favorable than that of a perfectly matched sequence, a lower analytical signal indicates a mismatch. Fluorescence is the detection method of choice for many highly selective assays that aim to detect a single base mismatch at concentrations of 50 nM [20], 10 nM [21] and most recently 0.26 fM[22]. A number of label-free methods for SPM detection have also been reported, including resonator arrays [23], silicon nanowires [24] and colorimetric detection with gold nanoparticles [12, 25-28], and these have been associated with limits of detection (LOD's) of 1.95 nM, 1 nM and 50 fM, respectively. However, they involve relatively lengthy assay times (1-4 hours), are destructive to the sample, require cumbersome instrumentation, and/or specialized fabrication techniques.

In the development of any new genetic analysis methodology, the aim is to provide a rapid analysis time with good sensitivity at a low cost. The IDEAL assay has the best balance of cost, speed and sensitivity, and that balance is usually defined by the application. The playoff between these three parameters almost always translates to compromise in one parameter at the expense of improving another. This applies to detecting SPM's in a rapid, cost-effective manner

for application to genome-based assays pertinent to diagnostic and pharmacogenetic tests that could be carried out in a point-of-care setting (i.e., using a microdevice). Hybridization assays have been adapted to microdevices in a number of embodiments since their genesis in the early 1990's [29-32]; attractive features driving this have been purported in numerous publications over the last two decades and include portability, reduced cost and rapid time-to-result. Microarray devices exploiting fluorescence detection provide such an abundance of genetic information (typically fabricated with 2-4 million probes sites [33]) that the bottleneck becomes the bioinformatic component. This technology has been shown applicable in a number of arenas (e.g., monitoring the effect of environment on cancer growth[34]); however, due to complex data processing, high expense and fluorescence microscopy, it is not applicable to rapid point-of-care SPM detection. Simplified label-free detection using PMPs as the probe substrate should be capable of providing rapid SPM detection and, ideally, integratable for end-point detection into micro-total analysis systems (μTAS).

We recently reported a new approach for detecting DNA hybridization events through a hybridization-induced aggregation (HIA) of particles [35]. Specifically, the aggregation of a pair of micron-scale oligonucleotide-adducted magnetic particles is induced by the hybridization of a complementary target DNA sequence that serves to tether the particles together (**Fig. 1A**). This allows for visual detection to be used as a qualitative indicator of hybridization, with more sensitive detection obtained by optical imaging, and processing of those images by a simple algorithm[35] (see **Fig. 1D**).

HIA is performed in a homogenous, chaotic system, where the probe-conjugated magnetic particles and target DNA are in constant motion due to the forces provided from a rotating magnetic field (RMF) and a vortexer (see **Fig. 1B**). Understanding the nuance factors

that affect hybridization in this chaotic environment is paramount to honing HIA as the end-point detection in a microfluidic detection system. In this report, we describe a systematic approach for understanding the fundamental character of oligonucleotide-adducted magnetic particle aggregation, and the subtleties of the target sequence prerequisites for optimal detection. Of particular importance is the understanding the effects of variations in the target sequence, since the design of the target sequence is often limited by the techniques used to prepare the DNA from *bona fide* samples for detection; for example, restriction enzyme digestion or PCR may result in a target sequence with non-complementary bases flanking the target region. In this study, we investigate the relationship between target sequence (and its variations) and hybridization efficiency, as measured by the aggregation response; included in these are the effect of non-complementary bases flanking the target region, the optimal length of the target sequence, and the ability of HIA to detect single point mismatch(es) in a DNA target sequence of a particular length. Finally, with a view to the future, HIA is shown to be effective in the presence of potential small molecule interferents that may be encountered in an integrated assay on a single microfluidic device.

Materials and Methods

Reagents

Dynabeads MyOne Streptavidin C1 1μm paramagnetic particles were purchased from Invitrogen (Carlsbad, CA) and were prepared in accordance with manufacturer's instructions. Biotinylated and unfunctionalized oligonucleotides were purchased from Eurofins MWG Operon (Huntsville, AL). Hydrochloric acid, sodium chloride, potassium chloride, and ethanol, were purchased from Fisher (Fair Lawn, NJ). 2-Amino-2-(hydroxymethyl)- 1,3-propanediol (Trizma base, 99.9%) and bovine albumin serum was purchased from Sigma (St. Louis, MO). Proteinase K, RNase 1 and 25 mM $MgCl_2$ was purchased from Life Technologies™ (Grand Island, NY). All solutions were prepared in Nanopure water (Barnstead/Thermolyne, Dubuque, IA).

Assay Instrumentation

Images of the microwells were collected by using a T1i DSLR camera with MP-E 65 mm f/2.8 1−5× macro lens purchased from Canon U.S.A., Inc. (Lake Success, NY). A Thermix Stirrer model 120S magnetic stir plate was purchased from Fisher Scientific (Fair Lawn, NJ). Three, 5-mm x 5-mm cylinder neodymium magnets were purchased from Emovendo (Petersburg, WV). A MS3 basic vortexer was purchased from IKA (Wilmington, NC). A Ledu compact desk magnifier lamp was purchased from Guy Brown Products (Brentwood, TN) and used without optics to provide lighting around the entire sample. Magnetic and vortexer rotation speeds were determined using a digital photo laser non-contact tachometer, purchased amazon.com.

Microwell Fabrication

A VersaLASER system 3.50 from Universal Laser Systems (Scottsdale, AZ) was used to fabricate microwells, cutting through 1.0 mm-thick PMMA purchased from Astra Products (Baldwin, NY). Each microwell device was prepared as a 4 × 4 matrix of 5-mm-diameter circular wells on a 4-cm square device, designed in AutoCAD. These were then thermally bonded using established methods[36] to a second 4-cm square 1.5-mm-thick PMMA, purchased from McMaster-Carr (Santa Fe Springs, CA). Microwells we sterilized in 2M hydrocholoric acid for 30 min, then rinsed with Nanopure water prior to use.

Assay Procedure

All assays were performed at room temperature (25°C), in a 5 mm PMMA microwell, with a 20 µL final volume: 17 µL of HIA buffer (10 mM Tris, 200 mM KCl, pH 7.5), 1 µL of probe-conjugated particles (particle concentration: 2 mg/mL), 1 µL of non-specific sequence and 1 µL of target DNA sequence. After adding the reagents, the microwell device was exposed to an RMF of 2000 rpm and a vortexing speed of 130 rpm for 12 minutes. A single picture was then taken of the microwell for analysis.

Results and Discussion

HIA is exciting because it is technically simple to execute (add DNA-containing sample and expose to a RMF) and has obvious potential for widespread applicability due to the visual (or optical) detection capability. However, in the original report we described the limitation associated with the instrumentation used (RMF only), in that only a single well could be optimally exposed to the RMF for effective aggregate formation. This limitation was overcome by modifying the hardware to incorporate a second (non-magnetic) force - agitation[37]. Notably, the use of agitation in the absence of the RMF results in aggregation responses that are highly irreproducible and only occur at micromolar target DNA concentrations. Combined with the RMF, however, this modification brought a substantial improvement to aggregation reproducibility in up to 16 wells (**Fig 1B,C**). The HIA aggregation response is semi-quantitative, meaning that the higher the concentration of target DNA in the assay, the greater the extent of aggregation. To quantify the extent of aggregation, each well is captured post-assay as a digital image, which is processed through an algorithm (in Mathematica™) to separate the particle pixels (dark) from the background (light) [35]. As shown in **Figure 1D**, the image is initially represented as *% Dark Area*, with completely non-aggregated particles (background; negative control) equaling the value of 100% Dark Area. For clarity, this scale was converted to describe the particle binding as *% Aggregation*. This value is given by the following equation:

$$(100 - \%\, Dark\ Area) + \ scaling\ factor = \%\, Aggregation$$

The 'scaling factor' is set so that maximum aggregation induced by the 'positive control' sample results in a value of 100% Aggregation. In the work presented here, a corrective scaling factor

of 8% was used, which set 100% Aggregation as the value for 10 μM (the highest concentration used) of the 26-mer target, which induced the most extensive aggregation observed with the initial target sequence. In addition, a non-specific control reaction containing 10 μM of a non-complementary 26-mer sequence was assayed to quantify nonspecific aggregation, and this provided the *threshold* for 'Minimum Aggregation', a value that baselined at ~10%, the same value as a DNA-free sample. Any aggregation value larger than this threshold was considered a 'positive' response and the target detectable. To demonstrate the specificity of HIA, 10 μM of this non-complementary sequence was added to each experiment as a negative control, unless otherwise stated.

The 26-mer target exploited in this work originated from a proximity ligation assay described in a previous report [38]. The target sequence is composed of a 20-base 'core region' that is complementary to the probe sequences, with a 3-base poly-A tail flanking the 5' end, and a 3-base poly-T tail flanking the 3' (**Fig. 2A, unmodified target sequence**). HIA assay parameters were considered optimized for this sequence when the aggregation values were distinguishable from the 10% baseline at the lowest detectable concentration of target DNA. The optimized conditions for aggregation induced by the 26-mer sequence included an applied RMF of 2000 rpm and a vortexer speed of 300 rpm. As seen in **Figure 2,** the 26-mer sequence was detectable at concentrations as low as 100 fM, representing a 100-fold improvement in sensitivity over a method with RMF only [35]. With this improvement the sensitivity, HIA is comparable to DNA hybridization detection methods with functionalized gold nanoparticles coupled with darkfield microscopy[39], electrochemical impedance spectroscopy[40] and SERS[41]. The effects of variation in the target sequence was explored by inducing base changes in the 20-base core region of the 26-mer target, while conserving the poly-AAA and poly-TTT tails on either side of the target

region. Due to the cost associated with the specific probe-particle combinations for any given target, base substitutions were restricted to the target with the sequence of the bead-bound probes unchanged.

The first set of modifications to the 26-mer involved the addition of 5, 10 or 15 additional bases on both sides of the core sequence (**See Figure 2A**). The additional bases were specifically designed to be non-complementary to the probes, yet maintain a GC content of ~50%. Each modified target sequence was assayed at a high concentration of 10 μM, with 10-fold serial dilutions carried out until the aggregation values were indistinguishable from the negative control, i.e., reached the minimum aggregation threshold of ~10%. The effect of the non-complementary flanking bases on the aggregation response is given in **Figure 2B**. There is a significant loss of sensitivity, as all of the modified sequences became undetectable at a concentration in the 0.1- 1.0 μM range. These results are consistent with hybridization theory, and confirm that the target sequence should be perfectly complimentary to the probe sequences, with no additional flanking bases for detection of low concentrations of DNA using the HIA assay. That said, HIA would still have utility for targets in the sub-nM range provided that the target sequence could be effectively amplified (i.e., PCR) or that restriction enzymes could be employed to trim the flanking bases so that as few non-complementary bases as possible remained.

The second investigation explored the effect of altering the length of the core probe-binding region of the target sequence. Five targets of different lengths were chosen to provide a varied sample set. Each utilized sequence retains a polyAAA- and polyTTT- segments flanking the core sequence. In addition to the original 20-base core sequence (of the 26-mer target), the following were tested: 12-mer (6-base core sequence), 16-mer (10-base core sequence), 32-mer

(26-base core sequence), and 38-mer (32-base core sequence). In order to make the length of target the only variable, the GC content for the probe-binding region for each sequence was maintained at roughly 60%. The structural differences between these target sequences are highlighted in **Table 1.** The most significant of these was an increase in melting temperature (T_m) with increasing target length (33 °C – 12-mer; 67 °C – 38-mer). This would obviously have detrimental effects for hybridization at room temperature, therefore, the 38-mer was chosen as the longest target sequence. In future designs for other targets, the significant differences in T_m, could be avoided, but this is difficult to avoid with short sequences. As shown in **Figure 3**, at the highest target concentration (10 μM), each sequence was readily detectable. The shortest targets (12-mer and 16-mer) were no longer able to induce an aggregation distinguishable from the negative control when the concentration was decreased 100-fold (100 nM). Both the 26-mer and 32-mer proved to be the most sensitive of the targets tested, yielding values still greater than 10% above the threshold at a target concentration as low as 100 fM, with a linear range of approximately 1 μM to 10 pM. The 38-mer, however, was not distinguishable above 1 pM. This is likely due to a higher T_m of the target sequence, with possible secondary structure of the target also contributing to loss of sensitivity. This indicates that the limit of detection (LOD; defined as the lowest concentration of target that results in an aggregation value above the 10% threshold) decreases with increasing target length up until ~26 bases. This trend is unsurprising considering the themodynamic gain contributed by each correctly paired base in a hybridization complex. The minimum LOD can be achieved with a target length between ~26 and 32 bases, after which increasing the length of the target results in an increase in LOD, presumably as a result of increased T_m. We hypothesize that it would be possible to achieve sensitive detection of longer

target sequences by increasing the hybridization temperature, which would require that the current instrumentation be augmented with a thermostatic control device.

We were interested in determining the effect of point mutations (PMs) on the ability of the 26-mer target to induce aggregation. This was an obvious next step since many mutation detection methods are based on hybridization techniques. As illustrated in **Figure 4A**, three test sequences were designed. The first test sequence contained a 10T→G substitution (replacing a pyrimidine with a purine) four bases from the probe junction. The mismatch location was chosen on the basis that maximum destabilization of a hybridized duplex has been reported to occur when a single base mismatch is located near the center of the target-probe binding complex [42]. A second substitution, a 17C→A, was inserted at a location that mirrored the first, i.e., four bases from the probe junction, to create a sequence with two mismatches. The third and final mismatch was located at the probe junction. A 12A→T substitution was specifically chosen for this in order to maintain the same % GC composition for both sequences containing multiple mismatches so that other effects, (e.g., bulging due to a G or C) could be to minimized (**Fig. 4A**). The aggregation response for these was evaluated at concentrations of 10 μM, 1 μM and 100 nM. At 100nM, the aggregation observed with all three target sequences plateaued at ~10%, and given this is threshold value, they were no longer distinguishable from the negative control (**Fig. 4B**). The sequence containing three mismatches was only detectable at high concentrations (10 μM), and even then, yielded an aggregation response that was low (~50%) relative to the sequence containing two mismatches. The sequence with two mismatches was detectable at μM concentrations, however, aggregation response dropped from ~55% to threshold (~10%) between 1 μM and 100 nM target concentrations. The same trend was observed for the sequence containing a single mismatch, which dropped from ~70% Aggregation to ~15% over the same

concentration range. These data highlight that the extent of destabilization of the hybridization duplex is proportional to the number of mismatches in the sequence, significantly reducing the LOD for aggregation compared to a fully-complementary sequence. We believe that the chaotic nature of the RMF-agitation system intensifies the destabilization of the complex, accounting for the loss of selectivity at lower target DNA concentrations.

As a result of the data in **Figure 4**, it is clear that single base mismatches can be revealed by a decrease in the extent of aggregation, and therefore HIA can be an effective method for mutation detection. The capability of detecting a single-base mutation detection is of particular significance for diagnostics, e.g., detection of the G20 19S mutation associated with Parkinson's disease[43]. For such applications, a HIA assay using bead adducted probes that are fully complementary to the wild-type sequence, would allow a mutation to be revealed simply by a decreased aggregation response. Additionally, it is interesting that, at micromolar concentrations, the extent of aggregation for 0, 1, 2 or 3 mismatches is distinguishable. This suggests that, at a defined target DNA concentration, HIA could potentially be used to determine the number of mismatches present in a given target.

The integration of HIA as the detection modality into a microdevice that also carries out the sample preparation is alluring, and is a natural progression towards novel and inexpensive sample-to-result system for DNA detection [44]. With the potential to exploit the HIA detection system for a variety of applications, it was important to evaluate the robustness of HIA in the presence of potential interferents based on their potential contamination to HIA from upstream sample processing. A list of nine conceivable interferents were amassed for evaluation based on their propensity to be involved in, 1) PCR mixtures: 25 mM $MgCl_2$ and 1.15/11.5/115 μg/μL bovine serum albumin (BSA) or 2) reagents common in DNA preparation: 20 μg/μL Proteinase

K, lysed blood, lysate and lysate RNase from a buccal swab. For evaluation of each of the nine reagents, the assay was carried out with a 1 μL aliquot from stock solutions (at the stated concentrations above), with and without the 26-mer target sequence (at 10 μM). Note that these experiments did not contain 1 μL of the non-complementary 26-mer sequence and, therefore, the volume of buffer remained the same. The results are given in **Figure 5**. In summary, two interferents – BSA and lysed whole blood – induced false aggregation, while none of the reagents inhibited the binding of the target DNA sequence.

BSA was evaluated at three concentrations (1.5, 11.5 and 115 μg/μL); with all of these, false aggregation was observed, and this is likely mediated though particle coupling via protein-protein interactions. Interestingly, at 115 μg/μL there was a reversal in this trend, with reduced false aggregation (relative to the 11.5 μg/μL concentration). Previous studies [45] have shown that albumin will bind DNA at high concentrations through hydrogen bonding, overcoming protein-protein interactions (e.g., between the BSA and avidin). Therefore, at high concentrations (115 μg/μL), it's possible that BSA binds the probes, reducing the extent of protein-protein binding and causing a reduction in false aggregation. Despite the effect at all BSA concentrations tested, this is not a problem for the HIA method because use of BSA in PCR master mix reagents (for surface passivation or polymerase stabilization) is typically at a concentration below 100 pg/μL.

The second interferent to produce false aggregation was lysed whole blood (75% Aggregation), which was expected due to protein-protein interactions of proteinaceous blood components with the particle-bound avidin [46]. Again, this is not likely to be a problematic interferent for two reasons: 1) whole blood cannot be used as a direct sample for specific DNA detection due to the length of genomic DNA; and 2) as a post-PCR detection step, whole blood components would have been removed in the DNA clean-up phase. All other interferents investigated here failed to

induce significant false aggregation that would detrimentally affect target DNA detection. This demonstrates the HIA can function as end point detection in an integrated microfluidic system, without loss of signal due to upstream interferents.

Conclusions

Through modifying the system hardware to utilize a RMF and agitation simultaneously, we demonstrated a 100-fold improvement in sensitivity and increased the throughput of our hybridization-induced particle aggregation. A systematic investigation into the effect of target composition on HIA was achieved by comparing the aggregation response of a 26-mer target DNA with subtle changes in sequence. The results show that a target sequence composed of 26 bases provides the most effective aggregation, and can be detected at femtomolar concentrations, although as few as six complementary bases will induce detectable aggregation. The addition of non-complimentary bases flanking the core probe-binding region of the target sequence was found to decrease the aggregation response and, therefore, sensitivity. With only five additional bases added to each end of the core sequence, the sensitivity was reduced to nanomolar concentrations. The ability of HIA to detect a single point mutation adds bandwidth to this method, especially with the preliminary demonstration here that target sequences containing 1-, 2- or 3-base mismatches could be distinguished. Importantly, at sub-nanomolar target concentrations, only the fully-complimentary sequence is detectable; thus, potentially demonstrating the required specificity for genetic-based diagnostics. Finally, effective HIA in the presence of potential interferents provides a glimpse into assay bandwidth. Not surprisingly, the physiological conditions required for hybridization invites binding-induced interference from high concentrations of BSA or whole blood lysate, thus, these should be avoided. However, the sample preparation steps likely to be employed prior to HIA minimize the likelihood that these would be present at anything approaching detrimentally contaminating concentrations (i.e., significantly lower than those tested). Moreover, none of the interferents inhibited bead hybridization of the target DNA, opening up the spectrum of applications that can be considered.

It is clear that, in order to maximize the potential impact of HIA for genetic analysis, integration with specific target amplification through PCR in a microfluidic could make this a powerful detection modality. These efforts are currently underway.

References

1. E. M. Southern, *Journal of Molecular Biology*, 1975, **98**, 503-517.
2. G. Jiang, A. S. Susha, A. A. Lutich, F. D. Stefani, J. Feldmann and A. L. Rogach, *ACS Nano*, 2009, **3**, 4127-4131.
3. X. Zuo, F. Xia, Y. Xiao and K. W. Plaxco, *Journal of the American Chemical Society*, 2010, **132**, 1816-1818.
4. M. Kumar and P. Zhang, *Langmuir*, 2009, **25**, 6024-6027.
5. J.-M. Nam, S. I. Stoeva and C. A. Mirkin, *Journal of the American Chemical Society*, 2004, **126**, 5932-5933.
6. S. I. Stoeva, J.-S. Lee, C. S. Thaxton and C. A. Mirkin, *Angewandte Chemie*, 2006, **118**, 3381-3384.
7. A. Barhoumi and N. J. Halas, *Journal of the American Chemical Society*, 2010, **132**, 12792-12793.
8. F. Gao, J. Lei and H. Ju, *Analytical Chemistry*, 2013, **85**, 11788-11793.
9. Y. Huang, J. Zhu, G. Li, Z. Chen, J. H. Jiang, G. L. Shen and R. Q. Yu, *Biosens Bioelectron*, 2013, **42**, 526-531.
10. S. Pinijsuwan, P. Rijiravanich, M. Somasundrum and W. Surareungchai, *Analytical Chemistry*, 2008, **80**, 6779-6784.
11. Z. Gagnon, S. Senapati and H.-C. Chang, *Electrophoresis*, 2010, **31**, 666-671.
12. C. Sz-Hau, I. L. Kun, T. Chuan-Yi, P. Sheng-Lung, C. Yao-Chen, L. Yi-Rou, W. Jui-Ping and L. Chih-Sheng, *NanoBioscience, IEEE Transactions on*, 2009, **8**, 120-131.
13. Y. He, K. Zeng, A. S. Gurung, M. Baloda, H. Xu, X. Zhang and G. Liu, *Analytical Chemistry*, 2010, **82**, 7169-7177.
14. K. M. Hansen, H.-F. Ji, G. Wu, R. Datar, R. Cote, A. Majumdar and T. Thundat, *Analytical Chemistry*, 2001, **73**, 1567-1571.
15. E. L. S. Wong, E. Chow and J. J. Gooding, *Langmuir*, 2005, **21**, 6957-6965.
16. A. Tsourkas, M. A. Behlke, S. D. Rose and G. Bao, *Nucleic Acids Research*, 2003, **31**, 1319-1330.
17. K. Wendler, J. Thar, S. Zahn and B. Kirchner, *The Journal of Physical Chemistry A*, 2010, **114**, 9529-9536.
18. M.-L. Chan, G. Jaramillo, K. R. Hristova and D. A. Horsley, *Biosensors and Bioelectronics*, 2011, **26**, 2060-2066.
19. Y. Gao, L. K. Wolf and R. M. Georgiadis, *Nucleic Acids Research*, 2006, **34**, 3370-3377.
20. H. Zhang, M. Wang, Q. Gao, H. Qi and C. Zhang, *Talanta*, 2011, **84**, 771-776.
21. H. Liu, S. Li, L. Liu, L. Tian and N. He, *Biosensors and Bioelectronics*, 2010, **26**, 1442-1448.
22. H. Dong, C. Wang, Y. Xiong, H. Lu, H. Ju and X. Zhang, *Biosensors and Bioelectronics*, 2013, **41**, 348-353.
23. A. J. Qavi, T. M. Mysz and R. C. Bailey, *Analytical Chemistry*, 2011, **83**, 6827-6833.
24. G.-J. Zhang, J. H. Chua, R.-E. Chee, A. Agarwal and S. M. Wong, *Biosensors and Bioelectronics*, 2009, **24**, 2504-2508.
25. S. Sorgenfrei, C.-y. Chiu, R. L. Gonzalez, Y.-J. Yu, P. Kim, C. Nuckolls and K. L. Shepard, *Nat Nano*, 2011, **6**, 126-132.
26. C. S. Thaxton, D. G. Georganopoulou and C. A. Mirkin, *Clinica Chimica Acta*, 2006, **363**, 120-126.
27. J. K. F. Wong, S. P. Yip and T. M. H. Lee, *Small*, 2012, **8**, 214-219.
28. X. Xu, W. L. Daniel, W. Wei and C. A. Mirkin, *Small*, 2010, **6**, 623-626.
29. J. B. Lamture, K. LBeattie, B. E. Burke, M. D. Eggers, D. J. Ehrlich, R. Fowler, M. A. Hollis, B. B. Kosicki, R. K. Reich, S. R. Smith, R. S. Varma and M. E. Hogan, *Nucleic Acids Research*, 1994, **22**, 2121-2125.

30. T. M.-H. Lee, M. C. Carles and I. M. Hsing, *Lab on a Chip*, 2003, **3**, 100-105.
31. Z. H. Fan, S. Mangru, R. Granzow, P. Heaney, W. Ho, Q. Dong and R. Kumar, *Analytical Chemistry*, 1999, **71**, 4851-4859.
32. P. Liu, R. J. Meagher, Y. K. Light, S. Yilmaz, R. Chakraborty, A. P. Arkin, T. C. Hazen and A. K. Singh, *Lab on a Chip*, 2011, **11**, 2673-2679.
33. N. V. Dharia, A. B. S. Sidhu, M. B. Cassera, S. J. Westenberger, S. E. R. Bopp, R. T. Eastman, D. Plouffe, S. Batalov, D. J. Park, S. K. Volkman, D. F. Wirth, Y. Zhou, D. A. Fidock and E. A. Winzeler, *Genome Biology*, 2009, **10**.
34. S. Bech, T. Petersen, A. Nørremølle, A. Gjedde, L. Ehlers, H. Eiberg, L. E. Hjermind, L. Hasholt, E. Lundorf and J. E. Nielsen, *Parkinsonism & Related Disorders*, 2010, **16**, 12-15.
35. D. C. Leslie, J. Li, B. C. Strachan, M. R. Begley, D. Finkler, L. A. L. Bazydlo, N. S. Barker, D. M. Haverstick, M. Utz and J. P. Landers, *Journal of the American Chemical Society*, 2012, **134**, 5689-5696.
36. Y. C. K. Yi Sun, Nam-Trung Nguyen, *Journal of Micromechanics and Microengineering*, 2006, **16**.
37. D. A. Nelson, B. C. Strachan, H. S. Sloane, J. Li and J. P. Landers, *Analytica Chimica Acta*, 2014, **819**, 34-41.
38. M. Gullberg, S. M. Gústafsdóttir, E. Schallmeiner, J. Jarvius, M. Bjarnegård, C. Betsholtz, U. Landegren and S. Fredriksson, *Proceedings of the National Academy of Sciences of the United States of America*, 2004, **101**, 8420-8424.
39. R. Verdoold, R. Gill, F. Ungureanu, R. Molenaar and R. P. H. Kooyman, *Biosensors and Bioelectronics*, 2011, **27**, 77-81.
40. A. A. Ensafi, M. Taei, H. R. Rahmani and T. Khayamian, *Electrochimica Acta*, 2011, **56**, 8176-8183.
41. M. Liu, Z. Wang, S. Zong, R. Zhang, D. Zhu, S. Xu, C. Wang and Y. Cui, *Analytical and bioanalytical chemistry*, 2013, **405**, 6131-6136.
42. F. Lucarelli, G. Marrazza and M. Mascini, *Analytica Chimica Acta*, 2007, **603**, 82-86.
43. C. Paisán-Ruíz, S. Jain, E. W. Evans, W. P. Gilks, J. Simón, M. van der Brug, A. L. de Munain, S. Aparicio, A. M. n. Gil and N. Khan, *Neuron*, 2004, **44**, 595-600.
44. C. J. Easley, J. M. Karlinsey, J. M. Bienvenue, L. A. Legendre, M. G. Roper, S. H. Feldman, M. A. Hughes, E. L. Hewlett, T. J. Merkel, J. P. Ferrance and J. P. Landers, *Proceedings of the National Academy of Sciences*, 2006, **103**, 19272-19277.
45. H. Malonga, J. F. Neault, H. Arakawa and H. A. Tajmir-Riahi, *DNA Cell Biol*, 2006, **25**, 63-68.
46. E. M. Phizicky and S. Fields, *Microbiological Reviews*, 1995, **59**, 94-123.

Figures:

Figure 1

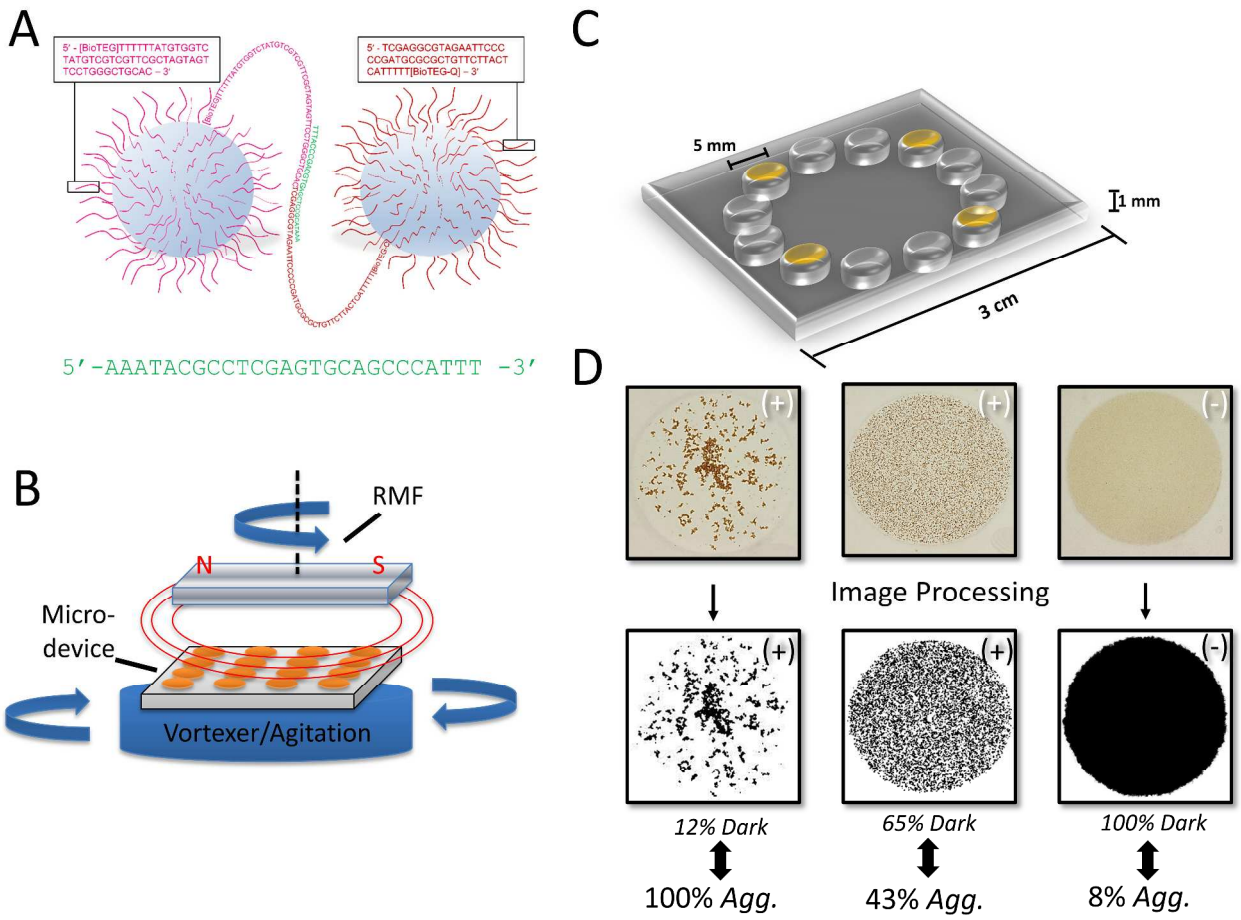

Figure 1: Scheme of HIA and instrument apparatus. ***A)*** *Cartoon representation of HIA, displaying the hybridization two different bead-bound ssDNA's by the complementary target sequence.* ***B)*** *The PMMA microdevice is contained in the vortexer, while the particles are magnetized by the RMF from above. The interaction of the particles with the free DNA in the microwell provides favorable kinetics for successful hybridization. C) Cartoon of the microdevice with four colored corner wells used for the assay.* ***D)*** *Photographs of HIA results converted into pixelated images for data processing to produce a measurable value for aggregation response. The results were normalized by applying the following equation: 100-Aggregation - %Dark Area + Scaling factor = % Aggregation. A scaling factor of 8% was applied.*

Figure 2

A

No. of flanking bases	Target sequence
0 (unmodified)	AAATACGCCTCGAGTGCAGCCCATTT
5	AAAGATCGTACGCCTCGAGTGCAGCCCAGATCGTTT
10	AAACTTAAGATCGTACGCCTCGAGTGCAGCCCAGATCGAATTCTTT
15	AAAGGTACCTTAAGATCGTACGCCTCGAGTGCAGCCCAGATCGAATTCCATGGTTT

B

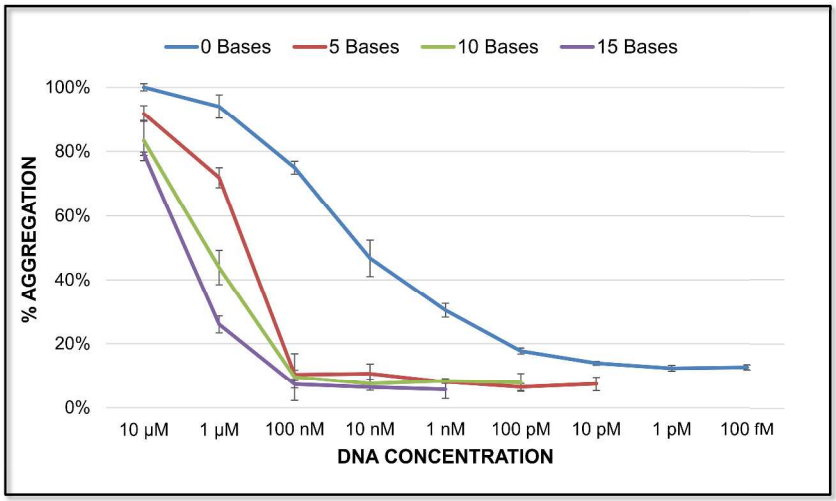

Figure 2: Effect of increasing the number of non complementary bases flanking the target sequence. A) Table highlighting the subtle differences in target sequence design for 0, 5, 10 and 15 non-complimentary flanking bases. B) Aggregation response of 5, 10 and 15 flanking bases is compared to the unmodified sequence.

Figure 3

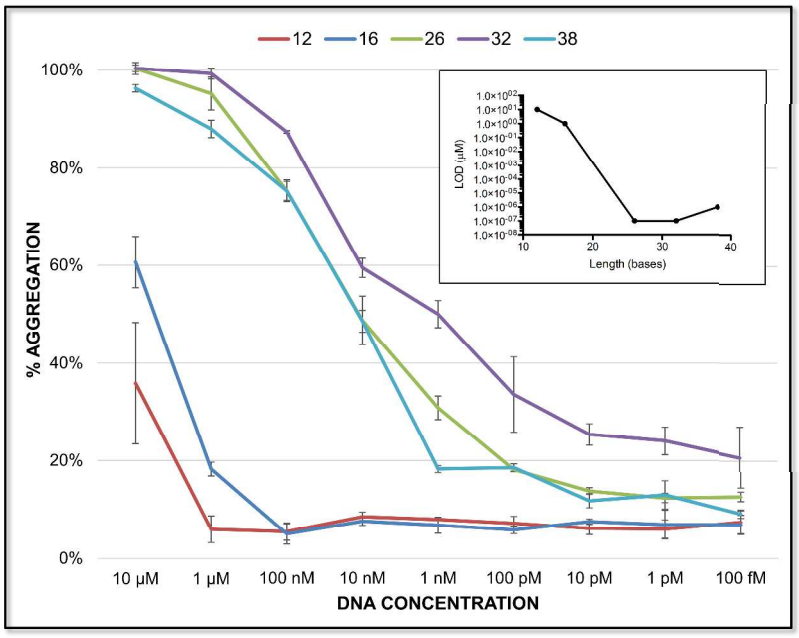

Figure 3: The effect on aggregation when the number of complimentary bases in the target strand is altered from to 12 to 38 bases. Inset: Plot of detection limit versus length of target sequence used.

Figure 4

A

No. of mismatches	Target sequence
0	AAA TAC GCC TCG AGT GCA GCC CA TTT
1	AAA TAC GCC GCG AGT GCA GCC CA TTT
2	AAA TAC GCC GCG AGT GAA GCC CA TTT
3	AAA TAC GCC GCG TGT GAA GCC CA TTT

B

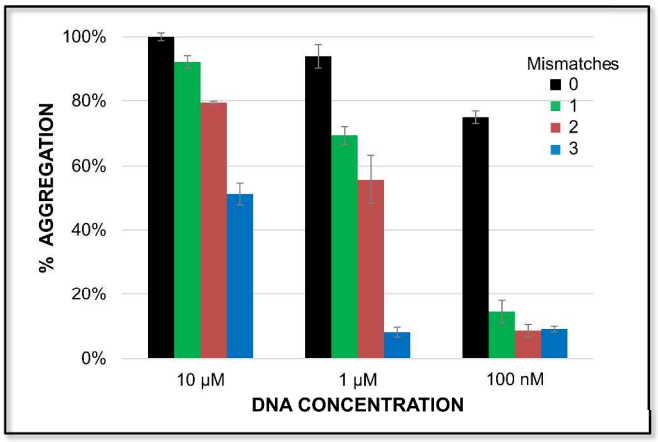

Figure 4: Detection of single point mutations through HIA. A) Sequences used to investigate the effect of aggregation from increasing SPM's. Purple and red bases illustrate the biotinylated probes. B) Results from using 10 μM – 100 nM of the target sequences. Aggregation response is compared to the sequence with no SPM.

Figure 5

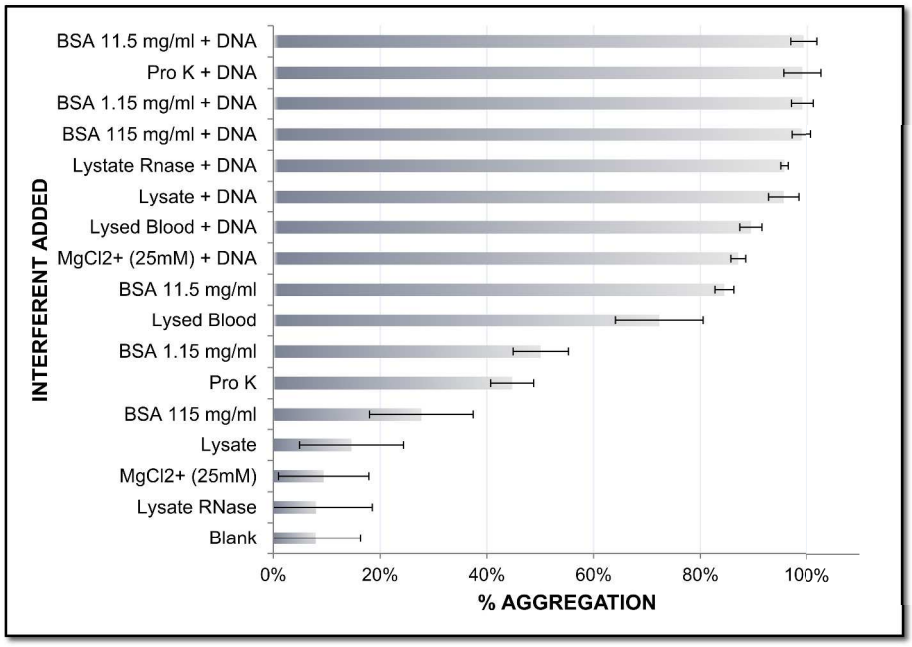

Figure 5: Evaluation of inducing false aggregation, or inhibition of DNA binding, with nine potential interferents during a theoretical integrated microdevice assay. Aggregation response is compared to the % Aggregation for the DNA alone.

Table 1

Table 1: Differences in the physical parameters associated with each sequence, highlighting the major differences between the shorter and longer targets.

Total length of target (bases)	Length of target–probe binding region (bases)	Target sequence	% GC binding	T_m (°C)
12	6	AAACGAGTGTTT	66.7	33.4
16	10	AAACTCGAGTGCATTT	60	45.5
26	20	AAATACGCCTCGAGTGCAGCCCATTT	65	62.8
32	26	AAATTCTACGCCTCGAGTGCAGCCCAGGATTT	61.5	65.6
38	32	AAAGAATTCTACGCCTCGAGTGCAGCCCAGGAACTTTT	56.3	66.7